WILEY | Hindawi

Research Article
Study on the Floating of Large Diameter Underwater Shield Tunnel Caused by Synchronous Grouting

Yu Liang [iD],[1] **Xumin Huang,**[2] **Shijun Gao,**[3] **and Yihao Yin**[3]

[1]School of Civil Engineering, Sun Yat-Sen University, Zhuhai 519000, China
[2]School of Aeronautics and Astronautics, Sun Yat-Sen University, Shenzhen 518000, China
[3]China Railway 14th Bureau Group Mega Shield Construction Engineering Co., Ltd., Nanjing 210000, China

Correspondence should be addressed to Yu Liang; liangyu25@mail.sysu.edu.cn

Synchronous grouting is the key factor causing segment floating during the construction of shield tunnel, especially the grout ratio and the control of the grouting pressure. In this paper, the ratio of grout material was optimized through multiple groups of physical and mechanical tests. The results showed that 0.3% content of water reducing agent in grout could improve the ability of water resistance significantly. 2.9% content of bentonite could reduce bleeding rate of grout and grout setting time and improve the fluidity in the meantime. Then, the distribution law of grout along the segment ring in the filling stage was studied based on a typical underwater tunnel in China. The results showed that the theoretical calculation of grouting pressure was between 0.15 MPa and 0.18 MPa, which were in good agreement with the measured data. The grouting pressure distribution is affected by four parts including the lateral earth pressure, foundation reaction, grout shear stress, and gravity.

1. Introduction

Shield tunnel has been widely used in traffic engineering crossing river and sea due to its advantages, and it tends to be larger in diameter and deeper in depth [1–3]. With the increase of the diameter of the shield tunnel, the buoyancy of the tunnel would be multiplied. During the process of shield tunnelling, a gap between the segment and the soil will occur after the segments come out from the shield tail [4, 5]. The segment tends to float upward due to the geological conditions and synchronous grouting [6, 7]. In particular, when the overlaying soil is shallow, segment floating is more prominent. For example, during the construction of underwater shield tunnels such as Dalian Road Tunnel (Shanghai), Yangtze River Tunnel (Shanghai), Qingchun Road Tunnel (Hangzhou), and Shiziyang Tunnel (Guangzhou) of China, the tunnel segments have appeared to varying degrees of buoyancy [4, 8, 9].

Another example is shown in Figure 1, which presented the floating situation of an underwater tunnel in China. The diameter of the tunnel is 13.8 m, and it passes through the stratum of silty clay, silty fine sand, and medium sand. Due to the large hydraulic conductivity of the sand layer and the abundant groundwater, serious floating of the segment occurs during construction.

The segment floating is often accompanied by segment damage and dislocation, and even the connection bolts could be cut off or lead to water leakage, which directly affects the safety of the tunnel construction, as shown in Figure 2. Therefore, it is necessary to study the mechanical action mechanism of shield tunnel and the reasons of tunnel uplift to ensure the safety of tunnel structure [10, 11].

2. Analysis of Floating Mechanism of Tunnel Segments

As known in Figure 1, serious segments floating occurred during shield tunnelling, segment installation, and synchronous grouting. The cumulative float of segments in some sections had exceeded the warning value, which will cause
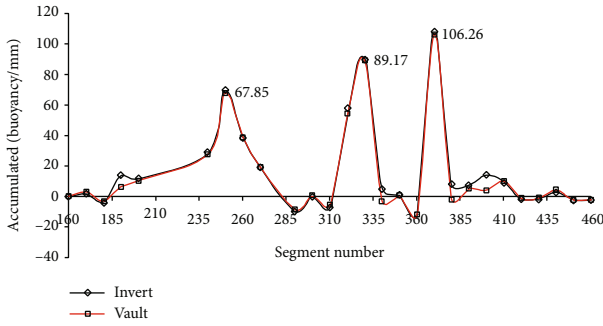
FIGURE 1: The floating situation of the underwater tunnel.

uneven stress on the segment, resulting in stress concentration and segment damage.

Many factors could affect tunnel floating, and these factors are often interrelated mutually such as geological conditions [6], synchronous grouting [12–14], and shield attitude control [15]. Based on the field monitoring data from the underwater tunnel mentioned above, two factors were discussed in this paper. The first factor is the change of surrounding rock properties. The underwater tunnel passed through many stratums including silty clay, silty fine sand, and medium sand. And the change of surrounding rock may lead to the change of rock strength and structural integrity. After shield excavation, the surrounding rock will not immediately fill the gap at the shield tail so that there is enough space for the segment to float. It is necessary to prepare grout with better fluidity, shorter setting time, and higher compressive strength when conducting synchronous grouting in this zone. The second factor is the control of the synchronous grouting. According to the construction record, the grout amount in the grout circulation system increased significantly when there is shield tunnelling through this area. Once the stratum conditions changed especially in the soft soil layer, the grouting pressure would be over large if the corresponding construction parameters were not adjusted in time. And then, the tunnel axis could deviate, resulting in segment floating.

Whether the construction control measures are appropriate has a great impact on the segment floating. In particular, when the stratum conditions are the same, the properties of the grout, grout buoyancy, and grouting pressure will have the greatest impact on it.

In this paper, the ratio of grout materials was optimized to improve the ability of water resistance and shorten the setting time. Then, the mechanism of grouting pressure in the filling stage was studied, and the flow law of grout along the circumferential direction in this stage was analyzed. Finally, taking the typical section of an underwater tunnel in China as an example, the distribution law of grout along the outer wall of segment and the floating situation of segment in the filling stage were verified, which would provide a theoretical reference for the floating control of segment in large diameter shield tunnel excavation in water-rich strata.

3. Study on the Properties of Synchronous Grouting Material

3.1. Performance Requirements of Underwater Synchronous Grouting. When synchronous grouting is carried out in the water-rich layer, the grout is easy to be lost from the layer with groundwater after spraying out, due to the poor water resistance. It is difficult to fill the gap of shield tail, resulting in the floating and leakage of the segment. For the water-rich layer with large hydraulic conductivity, synchronous grouting material requires the properties including fast filling, small bleeding rate, short setting time, good water resistance, and sufficient strength after the grout consolidation process is done. According to engineering experience, synchronous grouting material should meet the following requirements when shield tunnelling in water-rich layer area:

(1) Degree of fluidity: 230~250 mm

(2) Bleeding rate: 5%~10%;

(3) Setting time: 6~7 hours

(4) Shear strength: the 24-hour shear strength of grout should be greater than or equal to that of equivalent strata

(5) Compressive strength: the 7-day strength of grout should be greater than 0.50 MPa, and the 28-day strength of grout should be greater than 1.65 MPa

(6) Water resistance: a test method for the stability of grout in water was developed in this paper as shown in Figure 3. Firstly, put the test mold of grout into the water tank to make the water surface 10 cm above the mold. Connect it with the pipe and funnel, and inject the fresh grout into the mold until the grout overflows from the mold. Then, the mold and grout are placed in the water tank together to maintain until the specified time, and then, the grout is taken out for uniaxial compressive strength test. The water-land strength ratio is the strength ratio of grout with two different curing conditions (water and land) and with the same proportion at the same age after molding, so as to determine the water resistance of grout. The closer the water-land strength ratio is to 1, the better the water resistance of grout

3.2. The Optimization of Grout Ratio. According to the statistics of grout ratios in many similar projects, the commonly used water-binder (fly ash+cement) ratio ranges from 0.6 to 1, the binder-sand ratio ranges from 0.5 to 0.7, the bentonite-water ratio ranges from 0 to 0.2, and the fly ash-cement ratio ranges from 1.6 to 3.2. In order to reduce the test times, a series of physical mechanics and construction performance tests were carried out by using U15 (15^5) uniform design method [16]. Finally, a group of grout ratio was optimized as follows: cement 187 g, fly ash 313 g, bentonite 37.5 g, sand 770 g, and water 375 g. The test results of the grout ratio are shown in Table 1. Grout ratio 1 in the table is the one used in the tunnel at first, and ratio 2
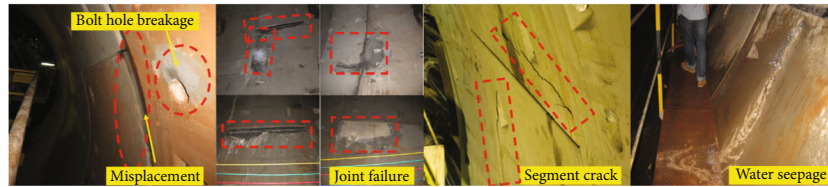
FIGURE 2: Segment damage during construction.

(a) Specimen preparation process

(b) Mortar specimen

FIGURE 3: The test of water resistance of grout.

was the optimized grout ratio mentioned above. The test results showed that ratio 2 effectively reduced the grout bleeding rate and improved the compressive strength, but the fluidity was too small and the solidification time was too long, so it was still not fully suitable for grouting in water-rich layers. In this paper, ratio 2 would be further optimized to meet the requirements of grout properties.

High-efficiency water reducing agent is a polymer surfactant with strong activity, which can be adsorbed on the surface of cement particles, forming a strong electric field to disperse cement paste and improving grout workability and strength. Besides, water reducing agent has no air entraining effect on cement and can improve the fluidity of cement under the same water amount effectively. Based on grout ratio 2, polyhydroxy acid water reducing agent (PHWR-S) was added to further improve its material performance. The grout specimen is shown in Figure 4. The left specimen was added with water reducing agent, and the right one was not. The specimen without water reducing agent was dark and grey, with fine particles on it. The grout specimen was greyish with water reducing agent and was smoother and uniform.

Too little addition of water reducing agent cannot shorten the initial setting time and improve strength of grout effectively, while excessive addition would cause waste and larger bleeding rate. The reasonable content of water reducing agent is about 0.3%, according to multigroup comparison test (ratio 3 in Table 1). Onshore and underwater compressive strength tests of ratio 3 were carried out and compared the test results with ratio 2. It can be seen from Table 1 that the initial strength of ratio 3 in land was slightly smaller than that of ratio 2, but the later strength increased rapidly. The strength of ratio 3 in water was greater than that of ratio 2, but the water resistance was not effectively improved.

The above tests showed that the active role of water reducing agent would improve the fluidity and reduce the setting time of grout. However, due to the increase of free water in the grout, the bleeding rate of the grout was higher than that without the water reducing agent, which may affect the overall performance of the grout.

To reduce the setting time and the bleeding rate of grout, the content of bentonite is increased without changing ratio 3 in Table 1. Based on the comparison of the field test, the reasonable content value was about 2.9%. Setting the number of the grout ratio with 2.9% bentonite as fourth. Compared with ratio 2, after adding water reducing agent and bentonite, the bleeding rate of grout was reduced to a certain extent, the fluidity of grout was improved, and the setting time of grout was further shortened, due to the unique sliding effect and water absorption of bentonite. The compressive strength of land and underwater changed little in the early stage of ratio 4, compared with ratio 3. But the 28-day compressive strength increased significantly later, and the water resistance was also improved. This showed that the addition of bentonite makes the grout structure more reasonable.

Based on ratio 4, the measured grout void ratio e_0 was 0.98 through specific gravity tests. The compression test of grout with ratio 4 was carried out to detect the compressibility of grout. After different curing time, the compression test results in the pressure range of 100 kPa-200 kPa are shown in Figure 5.

Figure 5 shows that the compressive modulus of grout increased slowly in the early stage and increased rapidly in the later stage. After 42.4 hours of curing, the compressive modulus of the improved grout was 24.4 MPa, which was similar to that of the layer (24.1 MPa) around the tunnel in the west bank of the river. However, the grout compression

TABLE 1: The test results of the optimized grout ratio.

Ratio number	Bleeding rate	Degree of fluidity (cm)	Initial setting time (h)	Compressive strength (7 d)	Compressive strength (28 d)	Water-land strength ratio (7 d)	Water-land strength ratio (28 d)
1	10%	28.1	8.5	0.71	/	Small*	/
2	5%	23.5	9.5	0.79	1.38	0.49	0.37
3	10.1%	26.0	8	0.65	3.66	0.86	0.36
4	6.6%	24.5	7	0.67	4.56	0.76	0.40

Notes: * means it is less than the instrument range.

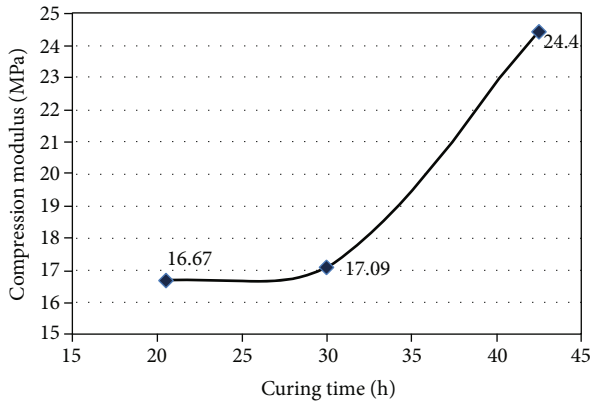FIGURE 4: The specimen with or without water reducing agent.

FIGURE 5: The change of the compressive modulus with the curing time.

modulus growth rate was slow. Therefore, when the shield crossed the stratum in the west bank, the tunnelling speed should be controlled as far as possible to ensure that no large settlement and deformation would occur.

4. Analysis of Grouting Pressure in Filling Stage

During shield tunnel construction, synchronous grouting can be divided into four stages including filling grouting, seepage grouting, compaction grouting, and fracture grouting. The filling grouting is at the stage of filling the gap of shield tail, which has the greatest impact on the segment floating. In the filling stage, grout filling along the circumferential direction and expansion along the longitudinal direction are considered to be two relatively independent processes. During synchronous grouting, it takes only a

few dozen seconds for the grout to fill along the circumferential direction to the farthest distance after ejecting from the grouting hole [17]. Relative to the speed of shield tunnelling, grout has enough time to form a three-dimensional annular "grout cake" along the circumferential shield tail gap, as shown in Figure 6. The longitudinal thickness δ of annular cake is much smaller than its width b, and its thickness is equal to the advancing distance of shield in the filling time. In the process of filling grouting, it is assumed that the grout only flows circumferentially along the shield tail gap without considering its longitudinal diffusion along the longitudinal direction.

Taking the horizontal direction of the segment ring as the x-axis, the vertical direction as the y-axis, and the tunnel axis as the z-axis, the spatial rectangular coordinate system was established as shown in Figure 7. In the diagram, α represents the angle between the grout filling position and the y-axis, and R represents the outer radius of the segment. The grout flow in the range of grouting hole 1 was taken as the research object. When the grout was sprayed from the grouting hole and filled downward, a microelement of the grout was studied [18].

Equation (1) can be obtained according to the force equilibrium. Thus,

$$Pbdz - (P + dP)bdz + \rho g \sin \alpha \cdot b \cdot \left(\frac{R+b}{2}\right) d\alpha \cdot dz$$
$$+ \tau b \left(\frac{R+b}{2}\right) d\alpha - (\tau + d\tau) b \left(\frac{R+b}{2}\right) d\alpha = 0, \quad (1)$$

where P is the filling pressure of the grout, τ is the shear stress, and ρ is the density of the grout. Since $b < <R$, it can be obtained that $R \approx (R + b)/2$. So, equation (1) can be simplified as follows:

$$d\tau = \frac{1}{R} \left(\rho g R \sin \alpha - \frac{dP}{d\alpha} \right) dz. \quad (2)$$

According to the boundary conditions, we can know that $\tau = 0$ when $z = 0$. The distribution formula of shear stress along the z-axis was obtained by integrating along the z-axis as follows:

$$\tau = \frac{z}{R} \left(\rho g R \sin \alpha - \frac{dP}{d\alpha} \right). \quad (3)$$
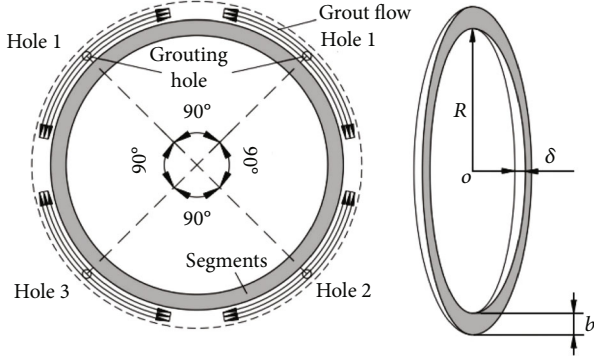
FIGURE 6: The grout filling the gap of shield tail along circumferential direction.
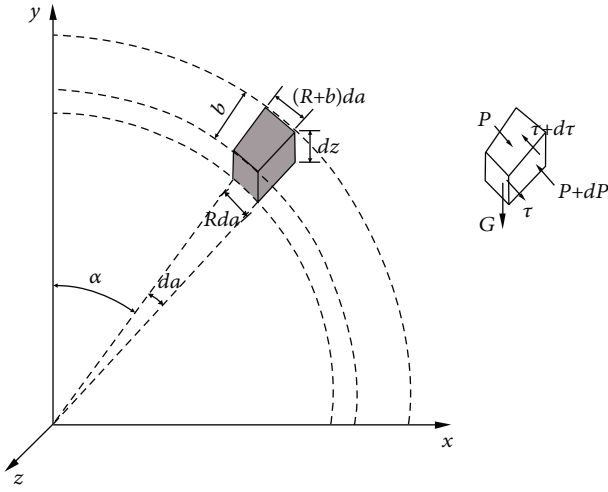

FIGURE 7: Model of grout filling and force analysis.

Let

$$\rho g R \sin \alpha - \frac{dP}{d\alpha} = B. \quad (4)$$

Then, equation (4) can be simplified to equation (5) as follows:

$$\tau = \frac{Bz}{R}. \quad (5)$$

Based on the test results by Ruan [19], it was assumed that cement grout is Bingham fluid in filling stage. The shear stress of the grout can be expressed:

$$\tau = \tau_0 + \mu\gamma = \tau_0 - \mu\frac{dv}{dz}, \quad (6)$$

where τ_0 is the shear stress of grout in static stage, μ is the grout viscosity coefficient, v is the flow speed of the grout, and γ is the shear rate. Substituting equation (5) into equation (6), equation (7) can be obtained:

$$dv = \frac{1}{\mu}\left(\tau_0 - \frac{Bz}{R}\right)dz. \quad (7)$$

Let $\tau_0 = Bz/R$, in equation (5), the flow core radius of the grout can be expressed as

$$r_p = \frac{\tau_0 R}{B}. \quad (8)$$

The speed distribution of classical Bingham fluid is shown in Figure 8. When $|z| \leq r_p$, fluid moves forward smoothly without shear force. And when $r_p \leq |z| \leq \delta/2$, the whole fluid is in motion relative to the adjacent layer fluid due to shear force. According to the boundary conditions, we can know that when $z = \delta/2$, $v = 0$. By integrating equation (7) along the z-axis, the speed distribution of the grout in the range of $r_p \leq |z| \leq \delta/2$ was obtained as follows:

$$v = \frac{1}{\mu}\left[\frac{B}{2R}\left(\frac{\delta^2}{4} - z^2\right) - \tau_0\left(\frac{\delta}{2} - z\right)\right]. \quad (9)$$

By substituting z for r_p in equation (9), the flow speed of the grout in the range of $|z| \leq r_p$ can be obtained:

$$v_p = \frac{1}{\mu}\left[\frac{B}{2R}\left(\frac{\delta^2}{4} - r_p^2\right) - \tau_0\left(\frac{\delta}{2} - r_p\right)\right]. \quad (10)$$

In summary, the speed distribution of the grout along the z-axis can be obtained:

$$v = \begin{cases} \frac{1}{\mu}\left[\frac{B}{2R}\left(\frac{\delta^2}{4} - r_p^2\right) - \tau_0\left(\frac{\delta}{2} - r_p\right)\right] & -r_p \leq z \leq r_p, \\ \frac{1}{\mu}\left[\frac{B}{2R}\left(\frac{\delta^2}{4} - z^2\right) - \tau_0\left(\frac{\delta}{2} - z\right)\right] & r_p < |z| \leq \frac{\delta}{2}. \end{cases} \quad (11)$$

By integrating, the flow on the section was obtained:

$$q = b\int_{-\delta/2}^{\delta/2} v\,dz = \frac{b}{\mu}\left[\frac{2B}{3R}\left(\frac{\delta^3}{8} - r_p^3\right) - \tau_0\left(\frac{\delta^2}{4} - r_p^2\right)\right]. \quad (12)$$

By substituting equation (8) into equation (12), one-dimensional cubic equation about B can be obtained:

$$B^3 - \left(\frac{3R\tau_0}{\delta} + \frac{12R\mu q}{b\delta^3}\right)B^2 - \frac{4R^3\tau_0^3}{\delta^3} = 0. \quad (13)$$

B can be solved by equation (13). And combining equation (4), differential P can be expressed:

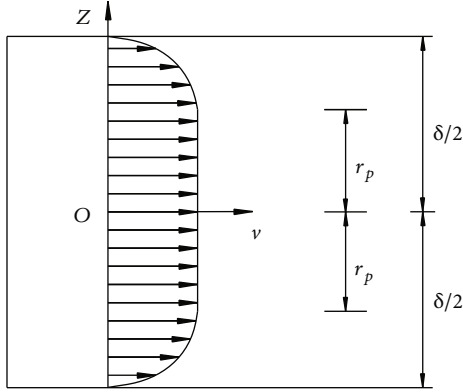$$dP = (\rho g R \sin \alpha - B)d\alpha. \quad (14)$$

FIGURE 8: The speed distribution of Bingham fluid.

When $\alpha = \alpha 1$, $P = P_1$ (P_1 is the actual grouting pressure for grouting hole 1). By integrating equation (14), the pressure distribution of the grout filling downward from grouting hole 1 can be obtained:

$$P = P_1 + \rho g R(\cos \alpha_1 - \cos \alpha) + B(\alpha_1 - \alpha). \tag{15}$$

Similarly, the pressure distribution of the grout filling upward from grouting hole 1 can be obtained:

$$P = P_1 + \rho g R(\cos \alpha_1 - \cos \alpha) - B(\alpha_1 - \alpha). \tag{16}$$

Let $\rho g R = A$. According to the above derivation, the grout pressure distribution of the ith grouting hole during filling stage can be obtained:

$$P = P_i + A(\cos \alpha_i - \cos \alpha) \pm B(\alpha_1 - \alpha), \tag{17}$$

where " + " represents the grout fills downward and "−" represents the grout fills upward.

5. Engineering Verification and Analysis

5.1. Grouting Pressure Monitoring and Verification. According to the above analysis, the grouting pressure in the synchronous grouting filling stage has a great influence on the floating of the segment. Taking the typical stratigraphic section of an underwater tunnel in China as an example, the grout buoyancy of the segment was calculated. Due to the short duration of filling stage, the influence of time varying of grout viscosity was not considered. The synchronous grouting hole at the tail of shield was arranged at the positions of 45°, 135°, 225°, and 315° respectively. And the grouting pressure at the outlet of grouting pipe was controlled at about 0.2 MPa.

The typical section of underwater tunnel is located at the bottom of the river. The surrounding strata of the tunnel are silty clay and silty fine sand. The relevant calculation parameters of stratum are shown in Table 2.

In order to understand the force variation of segments and the influence of synchronous grouting pressure on segment floating, pressure cells were set up in the typical stratigraphic section to monitor the fluctuation of grouting pressure and other external loads during shield tunnelling.

The typical pressure variation of the segments with time measured by the pressure cells is shown in Figure 9. The axial pressure immediately increased after the segment was removed from the shield tail. And then, due to the suspension of the shield tunnelling (replacement of the partial cutting tools on the cutter), the grouting behind the segment stopped, and the measured axial pressure decreased to about 0 rapidly. After normal tunnelling restarted, the measured axial pressure returned to the previous level. It was also proved from the measured curve that, after the segment was removed from the shield tail, the surrounding rock will not immediately act on the segment due to the good self-stability. A relatively complete gap in the shield tail will be formed around the segment, and the grouting pressure is the most important external load acting on the segment.

5.2. Calculation of the Grout Pressure Distribution. The main calculation parameters are listed in Table 3.

5.2.1. Thickness of the Ring Cake of Grout (δ). It is assumed that the grout is in a circumferential flow state within the range of thickness δ. According to the grout filling time and the shield tunnelling speed, the thickness of the flow ring cake can be express as

$$\delta = v_s t_0, \tag{18}$$

where v_s is the tunnelling speed of the shield and t_0 is the time required for the grout to fill the shield tail gap completely. Grout filling can be completed in about tens of seconds. If the parameter t_0 is 50 seconds, then $\delta = 0.0175$ m.

5.2.2. Sectional Flow (q). Four-hole synchronous grouting was adopted with the 0.2 MPa grouting pressure in each hole, and the injection rate is 150%. Assuming that the upward and downward filling flow from grouting hole is equal, the sectional flow q can be expressed as

$$\begin{aligned} q &= \frac{\pi\left[(R+b)^2 - R^2\right] v_s \lambda}{2n} \\ &= \frac{\pi\left[(5.65+0.165)^2 - 5.65^2\right] \times 0.00035 \times 150\%}{2 \times 4} \\ &= 3.9 \times 10^{-4} \text{ m}^3/\text{s}. \end{aligned} \tag{19}$$

5.2.3. The Pressure Distribution of the Grout (P). Substituting the relevant parameters into equation (17), the grouting pressure distribution along the outer wall of the segment in the filling stage can be obtained. Comparison between calculated and measured grouting pressure is shown in Figure 10. The theoretical calculation results were between 150 kPa and 180 kPa, which were in good agreement with the measured pressure on the vault, but the measured values on both sides of the arch waist and arch bottom were 50% larger than the calculated values. The pressure measured by the pressure cells was affected by the lateral earth pressure at the arch waist in addition to the grouting pressure. At the bottom

TABLE 2: Calculation parameters of surrounding strata.

(a) Silty clay

Unit weight γ_{mc} (kN/m³)	Cohesion c (kPa)	Internal friction angle φ (°)	Hydraulic conductivity q_{mc} (m/d)	Poisson's ratio μ	Static lateral pressure coefficient K_{mc}	Foundation coefficient (MPa/m)	Elastic modulus (MPa)
18	31.7	9.6	0.05	0.3	0.43	20.2	5.17

(b) Silty fine sand

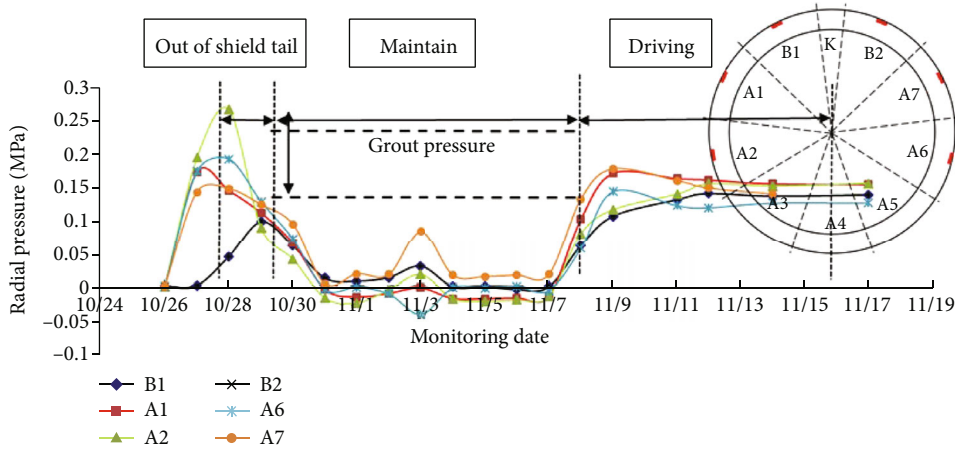| Unit weight γ_{mc} (kN/m³)	Cohesion c (kPa)	Internal friction angle φ (°)	Hydraulic conductivity q_{mc} (m/d)	Poisson's ratio μ	Static lateral pressure coefficient K_{mc}	Foundation coefficient (MPa/m)	Elastic modulus (MPa)
19	/	24	8	0.31	0.45	13	8

FIGURE 9: Measured axial pressure of the segment in typical section.

TABLE 3: The main calculation parameters of underwater tunnel.

Tunnelling speed (m/s)	Outer radius of segment (R/m)	Thickness of shield tail gap (m)	Grout density (kg/m³)	Plastic viscosity (Pa·s)	Dynamic shear force (Pa)
0.00035	6.9	0.25	1900	2	15

of the arch, it was mainly affected by the foundation reaction and the grout buoyancy caused by the concentration of liquid grout at the bottom.

5.3. Analysis of the Influence Factors. According to the calculation equation, the distribution and size of grout pressure along the segment are mainly affected by the grout weight (parameter A) and grout shear stress (parameter B). The gravity and shear stress of grout slow down the filling speed of grout when the grout is sprayed from bottom to top. When the grout is sprayed from top to bottom, the shear stress still slows down the filling speed, while the grout weight accelerates the filling process.

Substituting equation (19) into equation (13), it can be obtained:

$$B^3 - \left(\frac{3R\tau_0}{\delta} + \frac{12\pi R^2 \mu v_s \lambda}{\delta^3 n}\right)B^2 - \frac{4R^3\tau_0^3}{\delta^3} = 0. \tag{20}$$

The shear pressure (parameter B) is positively correlated with grout viscosity μ, grout injection rate λ, section area of segment ring πR^2, and shield tunnelling speed v_s, while negatively correlated with the thickness of grout cake δ (cubic). Parameter δ has the greatest influence on the shear pressure of the grout. When the other parameters are constant, δ is taken between 1 cm and 3.5 cm at 0.25 cm intervals. The
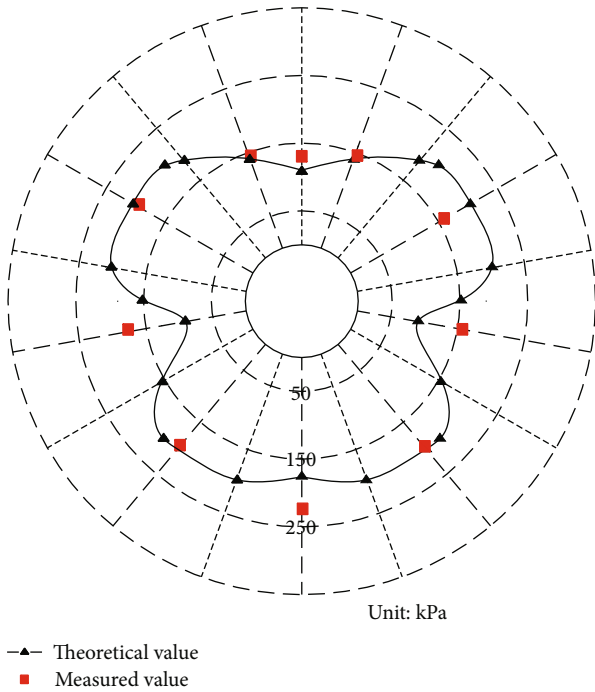
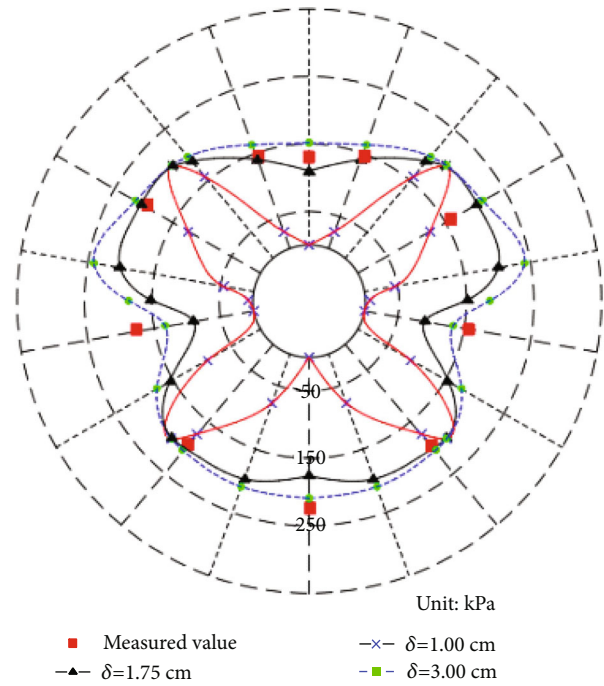FIGURE 10: Comparison between calculated and measured values of filling grouting pressure.

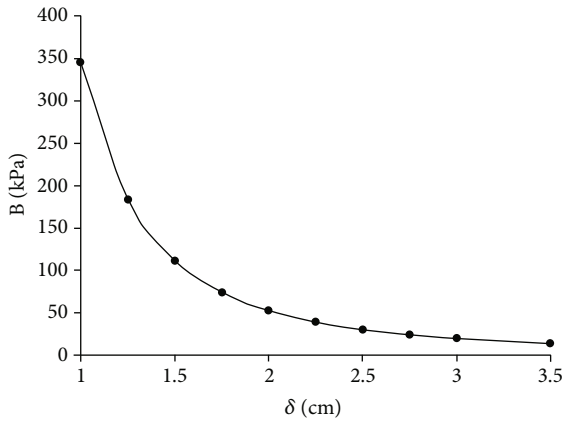FIGURE 12: Grouting filling pressure curve of Bingham fluid in different δ.

FIGURE 11: The relationship curve of parameter B with the change of δ.

relationship curve of parameter B with the change of δ is shown in Figure 11.

Parameters B increased sharply when δ was less than 2 cm, and when δ was larger than 3.5 cm, parameter B approached to 0. With the increase of the thickness of the grout annular cake, the grouting filling pressure c would decrease sharply. When δ was 1 cm, 1.75 cm, and 3 cm, respectively, the comparison between the calculated values and the measured values of grout filling pressure is shown in Figure 12.

Figure 12 shows that B was relatively large when δ was 1 cm. The shear resistance of grout was large, and the grouting pressure decays rapidly in the process of circumferential

filling. When the grout was filled to the vault and waist of the tunnel, the grouting pressure gradually decreased to 0. The calculated values were quite different from the measured values, which was obviously not in line with the actual situation. When δ was 1.75 cm and 3 cm, the corresponding B was relatively small with little difference according to Figure 11. The shear resistance of the grout was small, and the grouting pressure was evenly distributed along the whole ring. The measured values were basically in the two grouting pressure envelopes. Combined with Figure 12, it can be considered that the value of parameter δ under this condition was 1.75~3 cm.

Learned from the previous construction experience, corresponding adjustments had been adopted when excavating to the underwater section. Firstly, the tunnelling parameters had been adjusted in time according to the conditions of surrounding rock, so as to minimize overexcavation. Then, in the area with large floating amount, the tunnelling speed had been reduced relatively, and the binary grout with shorter setting time had been used for second grouting to fill the gap at the shield tail. The optimized ratio of grout had been used to reduce the fluidity and setting time of grout and ensure the quality of synchronous grouting. The cumulative floating and subsidence of the segments were controlled within 21 mm as shown in Figure 13, which ensured the safety and stability for the later tunnelling process. The maximum buoyancy was 20.47 mm, due to the change of the ground conditions. Compared with Figure 1, both buoyancy and settlement shown in Figure 13 were effectively controlled, especially the amount of uplift is significantly reduced.
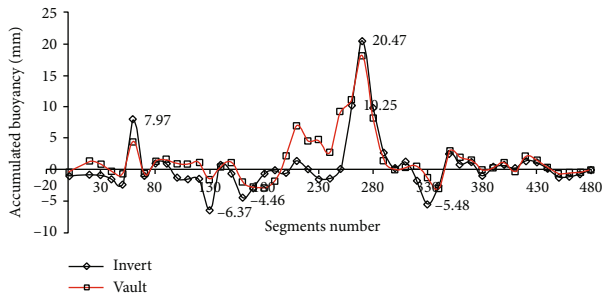
FIGURE 13: The deformation situation of underwater tunnel.

Compared with the floating situation of different segments in underwater tunnel, it is known that the synchronous grouting pressure is an important factor causing the floating of the segment, and it is also a key to control the floating of the segment. There are two conditions for segment floating: one is the space available for segment floating deformation, and the other is the force causing segment floating [20]. When the geological conditions change, the synchronous grouting parameters should be adjusted in time, the grout ratio should be optimized, and the synchronous grouting process should be optimized and controlled combining with secondary grouting and supplementary grouting.

6. Conclusion

In this paper, a test experiment was carried out to optimize the ratio of grout material. And then, the distribution law of grout along the outer wall of the segment in the filling stage was studied. The following conclusions can be drawn:

(1) In the test experiment of grout material ratio, 0.3% content of water reducing agent in grout could improve the ability of water resistance significantly. 2.9% content of bentonite could reduce bleeding rate of grout and grout setting time and improve the fluidity in the meantime

(2) The pressure distribution of grout along the outer wall was affected by gravity and grout shear stress. The gravity and shear stress of grout would slow down the filling speed of grout when the grout was sprayed from bottom to top. When the grout was sprayed from top to bottom, the shear stress still slowed down the falling speed of the grout, while the grout weight accelerated the filling process

(3) The typical stratigraphic section of underwater tunnel in China was taken as an example to verify the theoretical distribution law of the grouting pressure in the filling stage. The theoretical value was in good agreement with the measured one on the whole, but the errors of arch waist and arch bottom on both sides are relatively large. The errors were affected by the lateral earth pressure and foundation reaction

Data Availability

The data that support the finding of this study are available on request from the corresponding author. The data are not publicly available due to privacy or ethical restrictions.

Conflicts of Interest

The authors declare that they have no conflicts of interest.

Acknowledgments

References

[1] M. Q. Xiao, W. H. Sun, and X. Y. Han, "Research on upward moving of segments of shield segment," *Rock and Soil Mechanics*, vol. 30, no. 4, pp. 1041–1056, 2009.

[2] F. Zhang, Y. F. Gao, and Y. X. Wu, "Face stability analysis of large-diameter slurry shield-driven tunnels with linearly increasing undrained strength," *Tunnelling and Underground Space Technology*, vol. 78, pp. 178–187, 2018.

[3] Q. H. Qian and J. Chen, "Analysis of tunnelling risks of large-diameter shield and thoughts on its challenges," *Tunnel Constructions*, vol. 41, no. 2, pp. 157–164, 2021.

[4] A. M. Talmon and A. Bezuijen, "Calculation of longitudinal bending moment and shear force for shanghai Yangtze River Tunnel: application of lessons from Dutch research," *Tunnelling and Underground Space Technology*, vol. 35, no. 3, pp. 161–171, 2013.

[5] M. Theews and C. Budach, "Grouting of the annular gap in shield tunneling-an importance factor for minimization of settlements and production performance," in *Proceeding of World Tunnel Congress 2009*, Budapest, 2009.

[6] W.-C. Cheng, Z.-P. Song, W. Tian, and Z.-F. Wang, "Shield tunnel uplift and deformation characterisation: a case study from Zhengzhou metro," *Tunnelling and Underground Space Technology*, vol. 79, pp. 83–95, 2018.

[7] S. L. Shen, Y. J. Du, and C. Y. Luo, "Evaluation of the effect of rolling correction of double-o-tunnel shields via one-side loading," *Canadian Geotechnical Journal*, vol. 47, no. 10, pp. 1060–1070, 2010.

[8] X. Y. Zeng, Y. Liang, and K. Li, "Study on segment floating and its control measures during construction of large diameter cross river shield tunnel with shallow covering," *Railway Engineering*, vol. 57, no. 5, pp. 71–75, 2018.

[9] Y. Liang, J. Zhang, Z. S. Lai, Q. Y. Huang, and L. C. Huang, "Temporal and spatial distribution of the grout pressure and its effects on lining segments during synchronous grouting in shield tunnelling," *European Journal of Environmental and Civil Engineering*, vol. 24, no. 1, pp. 79–96, 2020.

[10] Z. Li, S. Zhou, H. Di, and P. Wang, "Evaluation and experimental study on the sealant behaviour of double gaskets for shield tunnel lining," *Tunnelling and Underground Space Technology*, vol. 75, pp. 81–89, 2018.

[11] S. Zhou, J. Xiao, H. Di, and Y. Zhu, "Differential settlement remediation for new shield metro tunnel in soft soils using corrective grouting method: case study," *Canadian Geotechnical Journal*, vol. 55, no. 12, pp. 1877–1887, 2018.

[12] A. M. Talmon and A. Bezuijen, "Simulating the consolidation of TBM grout at Noordplaspolder," *Space Technology*, vol. 24, no. 5, pp. 493–499, 2009.

[13] A. Bezuijen, A. M. Talmon, F. J. Kaalberg, and R. Plugge, "Field measurements of grout pressures during tunnelling of the Sophia Rail Tunnel," *Soils and Foundations*, vol. 44, no. 1, pp. 39–48, 2004.

[14] J. Liu, P. N. Li, L. Shi, J. Fan, X. Y. Kou, and D. Z. Huang, "Spatial distribution model of the filling and diffusion pressure of synchronous grouting in a quasi-rectangular shield and its experimental verification," *Underground Space*, vol. 6, no. 6, pp. 650–664, 2021.

[15] X. Xie, Q. Wang, I. Shahrour, J. Li, and B. Zhou, "A real-time interaction platform for settlement control during shield tunnelling construction," *Automation in Construction*, vol. 94, pp. 154–167, 2018.

[16] Z. Zhao, Y. G. Zhao, and P. P. Li, "Efficient approach for dynamic reliability analysis based on uniform design method and Box-Cox transformation," *Mechanical Systems and Signal Processing*, vol. 172, article 108967, 2022.

[17] Z. P. Fan, Y. W. Han, and Z. Q. Fang, "Calculation model of back filling grouting distribution for shield tunnel," *Journal of Highway and Transportation Research and Development*, vol. 28, no. 3, pp. 95–100, 2011.

[18] C. F. Gou, F. Ye, J. L. Zhang, and Y. P. Liu, "Ring distribution model of filling pressure for shield tunnels under synchronous grouting," *Chinese Journal of Geotechnical Engineering*, vol. 35, no. 3, pp. 590–598, 2013.

[19] W. J. Ruan, "Spread model of grouting in rock mass fissures based on time-varying behavior of viscosity of cement-based grouts," *Chinese Journal of Rock Mechanics and Engineering*, vol. 24, no. 15, pp. 2709–2714, 2005.

[20] W. R. Huang and W. B. Zhu, "To control the displacement of a shield tunnel during construction," *Modern Tunnelling Technology*, vol. 42, no. 1, pp. 71–76, 2005.